Research Square

Preprints are preliminary reports that have not undergone peer review.
They should not be considered conclusive, used to inform clinical practice,
or referenced by the media as validated information.

Myristoyl-modified BMAP-28m affects the cell cycle and apoptosis of prostate cancer cells by damaging the cell membrane

Meng Sun
Xinjiang Medical University
yunbo Zhang
Xinjiang Medical University
mengqi Zhang
Xinjiang Medical University
yimin Liu
Xinjiang Medical University
mengjia Li
Xinjiang Medical University
Yangyang Han
yyhan@xjmu.edu.cn

Xinjiang Medical University

Research Article

Keywords: Antimicrobial peptides, BMAP-28m, Cell cycle, Apoptosis, Mitochondrial damage

Posted Date: April 2nd, 2026

DOI: https://doi.org/10.21203/rs.3.rs-9156999/v1

License: This work is licensed under a Creative Commons Attribution 4.0 International License.
Read Full License

Additional Declarations: No competing interests reported.

Abstract

myr-BMAP-28m targeting of prostate cancer was developed by us in this study, to reveal the efficacy and principle of myr-BMAP-28m and compare BMAP-28m. It was found that compared with BMAP-28m, myr-BMAP-28m showed stronger cytotoxicity against prostate cancer cells than normal cells, thus yielding good tumor cell-targeting effect. Mechanistic study demonstrated that myr-BMAP-28m could arrest prostate cancer cells at the G1 phase, then induce apoptosis for prostate cancer cells with highly increased expression levels of apoptosis proteins. Its mode of action involves being attached to the cancer cell membrane, forming pores and penetrating into the cells, which results in an increase in lactate dehydrogenase (LDH) released from cells.Experiments including JC-1 staining, reactive oxygen species (ROS) detection, RHO123 staining, adenosine triphosphate (ATP) measurement, and scanning electron microscopy observation confirmed that myr-BMAP-28m could induce mitochondrial damage in cancer cells. In vivo experimental results showed that myr-BMAP-28m effectively inhibited the growth of prostate tumors with minimal adverse effects on host mice. Further verification via immunohistochemistry (IHC) assays indicated that after treatment with myr-BMAP-28m, the expression of apoptosis-related proteins was upregulated, while the expression of proliferation-related proteins was downregulated in tumor tissues. This study provides experimental evidence for the development of myr-BMAP-28m as a candidate drug for prostate cancer therapy.

Introduction

Prostate cancer (PCa) is the most common malignant tumor of the male urinary system, and its morbidity and mortality are among the highest in the world[1]. Early prostate cancer can be treated by surgery, radiotherapy, endocrine therapy and chemotherapy[2,3]. There are many limitations in the treatment of advanced or resistant prostate cancer, and chemotherapy drugs such as docetaxel are the main treatment[4,5]. However, the use of chemotherapy drugs has serious systemic side effects and multi-drug resistance, in addition to the strong heterogeneity of advanced tumors and the complex microenvironment[6,7], there is an urgent need to develop new treatment strategies with high efficiency and low toxicity.

Previous studies have shown that peptide drugs have positive effects on a variety of diseases. Antimicrobial peptides (AMPs) consisting of 5–50 amino acids not only possess broad-spectrum antimicrobial activity, but also show great anti-tumor potential in a variety of cancers[8,9]. Most antimicrobial peptides can destroy the integrity of the cell membrane of cancer cells through their cationic properties to achieve targeted lysis. Some antimicrobial peptides can regulate apoptosis-related pathways after penetrating the cell membrane. At the same time, it can also inhibit tumor by inhibiting angiogenesis and improving the tumor immune microenvironment[10–13]. Regardless of the potential anticancer mechanism, peptide-membrane interaction is necessary for antimicrobial peptides to play a role[14], which can be used to further study the positive effects of antimicrobial peptides on cancer treatment.

However, natural antimicrobial peptides have disadvantages such as instability, insufficient targeting and lipid solubility, which can be effectively improved by certain modifications[15–17]. Myristate modification, as an effective molecular modification strategy, not only improves the cell penetration of antimicrobial peptides by introducing lipid-soluble myristate groups, making it easier to cross the cancer cell membrane barrier to achieve an effective intracellular concentration, but also enhances the targeting selectivity of antimicrobial peptides to cancer cells and reduces the toxic side effects on normal cells[17,18]. At the same time, it further strengthens the anticancer activity of antimicrobial peptides, which can not only directly destroy the membrane structure of cancer cells to induce apoptosis, but also block the progress of cancer by regulating the tumor microenvironment and inhibiting tumor angiogenesis[19,20], providing a more potential candidate for cancer treatment.

In this study, myr-BMAP-28m was modified to enhance its anti-cancer effect, reduce its IC50 in cancer cells, and reveal the mechanism of its action in prostate cancer by myr-BMAP-28m, which has a high IC50 in cancer cells. It provides important theoretical and practical significance for promoting clinical translation, and provides experimental basis and theoretical support for the research and development of new therapeutic drugs.

Materials and Methods

Peptide Synthesis, Reagents and Instruments

myr-BMAP-28m, BMAP-28m (sequence: GGARSLGRKALRAWKKYGPAIVPIIRI) and Melittin (Mel, sequence: GIGAVLKVLTTGLPALISWIKRKRQQ) were stored as a stock solution in deionized water at -20°C and protected from light. The final product was purified using preparative reverse-phase high-performance liquid chromatography (RP-HPLC), resulting in a purity level greater than 98%. The peptide was uniquely tagged at the N-terminus with FITC, and its homogeneity was similarly above 98%.

Cell Culture

Du145 (Servicebio,China) was propagated in RPMI-1640 (G4535, Servicebio), and PC3 (Servicebio) was cultured in Ham's F-12 (G4562, Servicebio). HACAT and BPH-1 (Servicebio) were cultured in DMEM (G4511, Servicebio). All cells were cultured at 37°C, 5% CO_2, saturated humidity, 10% FBS (KF21, Royacel,China), and 1% penicillin/streptomycin (G4003, Servicebio).

Cell viability (MTT) assay

BMAP-28m and myr-BMAP-M at various concentrations was co-incubated with Du145, PC3, HACAT, and BPH-1 cells, and the cytotoxic effects were assessed using the MTT assay. In particular, 1×10^5 cells were plated in each well of 96-well plates. Du145 and PC3 cells were incubated with BMAP-28m and myr-BMAP-28m at concentrations of 0, 2, 4, 8, and 16 μM, while BPH-1 and HEEC cells were incubated with

BMAP-28m and myr-BMAP-28m at concentrations of 0, 10, 20, and 40 μM at 37°C for 24 hh. Then, the supernatant was removed, and 10 μL of MTT reagent (BS186, Biosharp, China) was added per well, followed by incubation at 37°C for 3 hh. Subsequently, 100 μL of dimethyl sulfoxide (A460700, Sangon Biotech, China) was added to each well and incubated under the same conditions for 30 min to promote the dissolution of any residual formazan product present in the wells. Afterwards, the absorbance was measured at a wavelength of 490 nm using Multiskan™ FC (51119000, Thermo Fisher, USA).

Trypan Blue Staining

Du145 and PC3 cell lines were seeded in 96-well plates at a density of 1×10^5 cells per well. Cells were cultured in appropriate media and treated with different concentrations of BMAP-28m or myr-BMAP-28m, while control groups included PBS and Mel treatments. After incubating for 24 hh at 37°C, 0.4% Trypan Blue dye (G1019, Servicebio, China) was added to the cell suspension and allowed to stain for 5 min. The cells were then washed three times with PBS and later analyzed under a fluorescence microscope (Eclipse Ts2, Nikon, Japan).

Hemolytic Activity Assay

Take 200 μL of fresh mouse blood and place it in a 1.5 mL EP tube containing sodium heparin. Centrifuge at 1200 rpm for 5 min, discard the supernatant, and resuspend the lower layer of red blood cells with 500 μL PBS. Mix thoroughly and centrifuge again at 1200 rpm for 5 min, then discard the supernatant. Repeat this procedure three times until the supernatant is clear. Dilute the volume to 3 mL, and add 0.1 mL to each well of a 96-well microplate. PBS serves as the negative control and Triton X-100 (BS084, Biosharp, China) serves as the positive control. Add different concentrations of BMAP-28m or myr-BMAP-28m (0, 2, 4, 8, 16, 32, 50 μM) to the wells. Incubate at 37 ℃ for 1 h, then centrifuge at 1000 rpm for 5 min. Transfer 50 μL of the supernatant from each well to a new 96-well microplate and measure the absorbance at 414 nm. Calculate the hemolysis rate of the antimicrobial peptide using the formula: $(A_{BMAP-28m/myr-BMAP-28m} - A_{PBS}) / (A_{Triton\ X-100} - A_{PBS}) \times 100\%$.

Peptide Binding Assay

The interactions of BMAP-28m and myr-BMAP-28m with Du145 and PC3 cell membranes were observed using high-content imaging technology. Cells were collected at a concentration of 1×10^6/ml and resuspended in PBS. Peptide binding activity was assessed by exposing the cells to FITC-BMAP-28m or FITC-myr-BMAP-28m at 37°C in the dark for 30 min. After incubation, cells were washed with PBS and then analyzed using a high-content imaging system (ImageXpress Confocal HT.ai, Molecular Devices, China). The average fluorescence intensity was measured for 10,000 cells per sample.

Cell Cycle Analysis

BMAP-28m was added to Du145 and PC3 cells at concentrations of 0, 2 μM and 0, 4 μM, respectively, while myr-BMAP-28m was added to Du145 and PC3 cells at concentrations of 0, 1 μM and 0, 1 μM, respectively, together with Mel (2 μM, as a positive control) and incubated for 24 hh. After treatment, cells were collected, washed with PBS, fixed with 70% ethanol, and then stained with 1 mg/mL PI (1246MG010, Biosharp, China), 0.1% Triton X-100 (BS084, Biosharp, China), and 100 μg/mL RNase A (BL543A, Biosharp, China). The samples were incubated at 37°C in the dark for 20 min, and DNA content was measured by flow cytometry (CytoFLEX LX, Beckman, USA). Appropriate gating was used to exclude debris and cell aggregates, and the different phases of the cell cycle (G1, S, and G2) were determined based on the FL3-A signal.

Annexin V/PI Staining Assay

Seed cells in 96-well plates at a density of 1,000 cells per well. BMAP-28m was added to Du145 and PC3 cells at concentrations of 0, 2, 4 μM and 0, 4, 8 μM, respectively, while myr-BMAP-28m was added to Du145 and PC3 cells at concentrations of 0, 1, 2 μM, respectively. 2 μM Mel was used as a positive control. After 24 hh of culture, remove the medium and wash the cells twice with PBS. Then, add 1 μL Annexin V-FITC and 1 μL PI to 100 μL binding buffer and mix thoroughly. After washing the cells once with PBS, stain with 10 μL Hoechst 33342 (BL1145, Biosharp, China) at room temperature for 5 min. After washing twice with PBS again, image and analyze the stained cells using a high-content imaging system (ImageXpress Confocal HT.ai, Molecular Devices, Sunnyvale, California, USA).

Lactate dehydrogenase (LDH) release

Lactate dehydrogenase (LDH) release was assessed according to the kit instructions (G1610, Servicebio, China). Du145 and PC3 cells were cultured at a concentration of 1 × 10^5/mL in RPMI 1640 and F12 media, respectively, and incubated at 37°C for 12 hh. Subsequently, the cells were treated with different concentrations of BMAP-28m or myr-BMAP-28m (0, 2, 8, and 20 μM) for 24 hh. PBS and 2% Triton X-100 served as control samples. After centrifuging the microplate, 100 μL of the cell-free supernatant was carefully transferred to another microplate. A mixture containing the tetrazolium salt reaction was added to each well, and the absorbance of the resulting colored formazan was measured at 490 nm using a Multiskan™ FC (51119000, Thermo Fisher, USA).**Scanning Electron Microscopy (SEM)**

PC3 cells were seeded onto round glass slides and incubated for 9 hh to allow attachment. After setting up control and myr-BMAP-28m treatment groups for 30 min, the cells were centrifuged, washed with PBS, and resuspended in electron microscopy fixative. The fixed samples were rinsed three times with 0.1 M phosphate buffer (pH 7.4, 15 min each) and then fixed in 1% osmium tetroxide (dissolved in 0.1 M phosphate buffer, pH 7.4) for 1–2 hh at room temperature in the dark, followed by another three washes. Dehydration was carried out sequentially using 30%–100% ethanol (15 min each) and isopentyl acetate (15 min). The samples were dried using a critical point dryer (K850, Quorum, UK), mounted on conductive carbon tape, and sputter-coated with gold for about 30 seconds using a sputter coater

(MC1000, HITACHI, Japan), then imaged using a scanning electron microscope (SEM, SU8100, HITACHI, Japan).

Transmission Electron Microscopy (TEM)

PC3 cells were seeded in 6-well plates and cultured for 9 hh to allow cell adhesion, then divided into a control group and a myr-BMAP-28m treatment group. After 24 hh of treatment, cells were harvested by trypsin digestion. The supernatant was discarded, and the cells were resuspended in an electron microscopy fixative. After removing the supernatant, 0.1 M phosphate buffer (PB, pH 7.4) was added. The cells were mixed, rinsed for 3 min, and centrifuged; this washing step was repeated three times. Samples were pre-embedded in agar, fixed, dehydrated, infiltrated, and embedded at room temperature. After polymerization, ultrathin sections were cut, stained, and imaged using a transmission electron microscope (HT7800, Hitachi, Japan).

Fluorescence Staining Analysis

Du145 and PC3 cells were seeded into 6-well plates containing sterile coverslips pre-coated with 1 mg/mL poly-L-lysine and cultured until the cells adhered. The adherent cells were treated with FITC-labeled BMAP-28m or myr-BMAP-28m for 1 h. Cells on the coverslips were fixed with 4% (w/v) paraformaldehyde (prepared in PBS). After thorough washing with PBS, the cells were incubated with Hoechst 33342 (1:1000 dilution) and Rho123 for 45 min. Images were acquired using a confocal laser scanning microscope (Ni-E C2, Nikon, Japan).

Experiment on Accumulation of Reactive Oxygen Species (ROS)

ROS accumulation was measured using a ROS detection kit (G1706, Servicebio, China). In Du145 and PC3 cells, the concentrations of BMAP-28m and myr-BMAP-28m were 0, 2, 4, and 8 μM, with an incubation time of 10 hh. Subsequently, cells were treated with DCFH-DA (10 μM) for 30 min in the dark. Fluorescence intensity was measured at 488 nm using a Multiskan™ FC (51119000, Thermo Fisher, USA) to assess ROS production.

ATP Content Detection

Cell viability was measured using the ATP bioluminescence cell viability assay kit (G1612, Servicebio, China). Du145 and PC3 cells were seeded in 96-well plates. After the cells adhered, BMAP-28m was added to the respective cells at concentrations of 0, 4, and 8 μM for Du145 cells and 0, 2, and 4 μM for PC3 cells, while myr-BMAP-28m was added to Du145 and PC3 cells at concentrations of 0, 1, and 2 μM. Then, 100 μL of the detection reagent was added to each well, gently shaken at room temperature for 1 minute, incubated for 3 min, and the luminescence intensity was measured using a chemiluminescent microplate reader (VICTOR Nivo, Revvity, USA).

JC-1 Analysis

Mitochondrial membrane potential (Δψm) changes were assessed using the JC-1 Mitochondrial Membrane Potential Assay Kit (G1515, Thermo Fisher, China). Briefly, BMAP-28m was added to Du145 cells at concentrations of 0, 4, and 8 μM, and to PC3 cells at concentrations of 0, 2, and 4 μM. myr-BMAP-28m was added to Du145 and PC3 cells at concentrations of 0, 1, and 2 μM, and incubated for 24 hh. Cells were then collected, washed with ice-cold PBS, and incubated with 10 μg/mL JC-1 dye at room temperature for 30 min. After incubation, the cells were washed with JC-1 wash buffer. Detection was performed using a high-content imaging system (ImageXpress Confocal HT.ai, Molecular Devices, China). During imaging, JC-1 monomers were excited at 490 nm, and emission was recorded at 530 nm. JC-1 aggregates were excited at 525 nm, and emission was measured at 590 nm.

Western Blot

BMAP-28m was added to Du145 cells at concentrations of 0, 4, and 8 μM, and to PC3 cells at concentrations of 0, 2, and 4 μM. myr-BMAP-28m was added to both Du145 and PC3 cells at concentrations of 0, 1, and 2 μM. Additionally, Mel was used at 2 μM as a positive control. The cells were then cultured for 24 hh. Cells were collected using radioimmunoprecipitation assay (RIPA) lysis buffer (P0039, Beijing Biotai, China) and centrifuged at 15,000 × g for 10 min. The resulting supernatant was then separated using 8–12% sodium dodecyl sulfate-polyacrylamide gel electrophoresis (SDS-PAGE) and subsequently transferred to a polyvinylidene fluoride (PVDF) membrane (ISEQ00010, Millipore, Germany). For blocking, the membrane was treated with 5% bovine serum albumin and then incubated with polyclonal antibodies specifically targeting Bcl-2 (WL01556, Wanleibio, China), Bax (WL01637, Wanleibio, China), Caspase3 (19677-1-AP, Proteintech, China), PARP1 (GB111500, Servicebio, China), β-actin (HA722023, Huabio, China). I ncubated with peroxidase-conjugate secondary antibodies. Membranes were visualized using Immobilon western chemiluminescent horseradish peroxidase substrate (BL520A, Biosharp, China), images were acquired by Azure 600 imaging system (CA94568, Azure Biosystems, USA).

Transplantation Tumor

Suspend 1×10^7 PC3 cells in 0.1 mL of PBS and subcutaneously inject them into both sides of BALB/c nude mice. Once the tumor size reaches approximately 100 mm^3, randomly allocate the mice into three groups (n = 6 in each group) and administer treatment continuously for 15 days following this scheme: Group 1: PBS (vehicle control), Group 2:BMAP-28m at a dose of 2.5 mg/kg, Group 3:myr-BMAP-28m at a dose of 2.5 mg/kg;Group 4: Melittin at a dose of 2.5 mg/kg. All treatments are administered via intraperitoneal injection on days 1, 4, 8, and 12. Monitor the body weight and measure the longest and shortest diameters of the tumors every three days, then calculate the tumor volume using the formula $V = \text{length} \times \text{width}^2 \times 0.5$. At the conclusion of the experiment, euthanize the nude mice. Measure both the volume and weight of the tumors, and take photographs. Furthermore, fix the tumors along with the major organs (heart, liver, spleen, lungs, and kidneys) in paraformaldehyde. Embed the fixed tissues in paraffin, remove the paraffin after sectioning, and conduct HE staining.

Paraffin-embedded tumor tissues from nude mice were cut into 5 μm-thick sections, dried, and deparaffinized with xylene. Subsequently, the sections were dehydrated with a graded ethanol series, washed, and subjected to antigen retrieval. The sections were then treated with 30 g/L hydrogen peroxide solution at room temperature for 30 min. After performing three washes with PBS, the primary antibodies specific to mouse Ki67 and Cleaved Caspase3 (1:300, Bioworld, China) were introduced and allowed to incubate for 1 h at 37°C. The sections underwent three washes with PBS, followed by the addition of a horseradish peroxidase-conjugated secondary antibody, which was incubated at 37°C for 30 min. After this incubation, the sections were taken out, and the nuclei were stained using a DAB chromogen kit (36302ES01, maxim, China). After counterstaining with hematoxylin for 2 to 5 min, the sections were dehydrated, mounted, and observed under an inverted fluorescence microscope (MF53-N, Mshot,China).

Result

1. Toxicity of myr-BMAP-28m against prostate cancer cells

To evaluate the cytotoxicity of myr-BMAP-28m against prostate cancer cells, Additionally, the hemolysis experiment revealed that although the hemolytic activity of myr-BMAP-28m was slightly higher than that of BMAP-28m, at a concentration of 50 μM, its hemolysis rate of mouse red blood cells was still lower than 40%, which was much higher than its IC50 value for prostate cancer cells, further supporting its favorable therapeutic window (Fig. 1F). In this study, the inhibitory activities of myr-BMAP-28m and BMAP-28m in two prostate cancer cell lines, PC3 and Du145, and two normal epithelial cells, BPH and HaCaT, were examined by MTT assay and trypan blue staining (Fig. 1A-B, E). Results showed that compared with BMAP-28m, myr-BMAP-28m significantly inhibited the proliferation of PC3 and Du145 cells in a concentration-dependent manner. The half maximal inhibitory concentration (IC50) of BMAP-28m against PC3 and Du145 cells was 2 μM and 4 μM, respectively, while the IC50 of myr-BMAP-28m in both cell lines was as low as 1 μM, indicating a stronger anti-tumor activity. "In contrast, the two peptides were less toxic to BPH and HaCaT normal epithelial cells, with IC50 values significantly higher than those in tumor cells (Fig. 1C-D), suggesting a selective killing effect on tumor cells." In addition, hemolysis experiments showed that although myr-BMAP-28m had slightly higher hemolytic activity than BMAP-28m, its hemolytic rate against mouse erythrocytes was still less than 40% at concentrations up to 50 μM, which was much higher than its IC50 value against prostate cancer cells, further supporting its favorable therapeutic window (Fig. 1F).

(A–D) CCK-8 assays showing dose-dependent viability of PC3 (A), Du145 (B), BPH-1 (C), and HACAT (D) cells after 24 h treatment with peptides (0–16 μmol/L). *n = 3, *$P < 0.05$, **$P < 0.01$, ***$P < 0.001$ vs. ctrl. (E) Transwell migration assays of PC3 and Du145 cells treated with peptides, showing reduced migration in a concentration-dependent manner. Scale bar: 200 μm. (F) In vivo antitumor efficacy of BMAP-28m and myr-BMAP-28m in PC3 xenografts. Tumor volume (% of control) after i.v. administration every 3 days for 21 days. *n = 6, *$P < 0.05$, **$P < 0.01$, ***$P < 0.001$.

2. Effects of myr-BMAP-28m on cell cycle, apoptosis and apoptotic proteins in prostate cancer cells

After 24 hh of treatment with BMAP-28m and myr-BMAP-28m on PC3 and Du145 cells, both BMAP-28m and myr-BMAP-28m induced a large number of cells to arrest in the G1 phase, and the effect of myr-BMAP-28m was more significant. The number of PC3 and Du145 cells arrested in the G1 phase induced by myr-BMAP-28m treatment (62.21%) was significantly higher than that induced by BMAP-28m treatment (46.44%) (Fig. 2A). To investigate whether myr-BMAP-28m induces apoptosis in PC3 and Du145 cells, we performed V-FITC/PI staining assays. myr-BMAP-28m significantly induced apoptosis in PC3 and Du145 cells in a dose-dependent manner, and could induce more apoptosis at a lower concentration compared to the BMAP-28m treatment group (Fig. 2B, Supplementary Fig. 1). Meanwhile, WB analysis was used to evaluate the effects of BMAP-28m and myr-BMAP-28m on the apoptotic pathway. As shown in the Figure, the expression levels of pro-apoptotic proteins Bax and Cleaved Caspase3 were significantly increased, while the expression level of anti-apoptotic protein Bcl-2 was decreased, and the expression level of PARP, which promotes DNA repair, was also significantly reduced in PC3 and Du145 cells treated with myr-BMAP-28m. Compared with the BMAP-28m treatment group, the changes in the myr-BMAP-28m treatment group were more significant (Fig. 2C, Supplementary Fig. 2).

3. Membrane binding and cleavage of prostate cancer cells by myr-BMAP-28m

myr-BMAP-28m targets and binds to prostate cancer cell membranes and induces damage. The LDH release experiment showed that in Du145 and PC3 cells, at 8 μM, the LDH release amount of the myr-BMAP-28m treatment group was significantly higher than that of the BMAP-28m treatment group, and with the increase of drug concentration and time, the LDH release rate significantly increased, showing a concentration and time-dependent relationship (Fig. 3D). High-content imaging results showed that the binding ability of the myr-BMAP-28m-treated cells was better at a lower concentration than that of the FITC-labeled BMAP-28m-treated cells. The binding of myr-BMAP-28m was dose-dependent, with about twice the binding intensity at high concentration compared with low concentration in Du145 and PC3 cell lines (Fig. 3A). Confocal microscopy results also confirmed that FITC-labeled myr-BMAP-28m could bind to the cell membrane of Du145 and PC3 cells, and with time, myr-BMAP-28m was translocated into the cells (Fig. 3B). Moreover, scanning electron microscopy (SEM) results showed that the cell surface perforations were observed in PC3 cells after treatment with myr-BMAP-28m. This suggests that myr-BMAP-28m may cause cell damage by binding to the membrane of prostate cancer cells (Fig. 3C). The LDH release assay showed that in Du145 and PC3 cells, the LDH release of the myr-BMAP-28m-treated group was significantly higher than that of the bMAP-28m-treated group at 8μM, and the LDH release rate was significantly increased with the increase of drug concentration and time. A concentration-time dependence was shown (Fig. 3D).

4. Effect of myr-BMAP-28m on mitochondria

To investigate the effects of myr-BMAP-28m on oxidative stress and mitochondria in prostate cancer cells, we first evaluated the changes in JC-1 in both cell types after myr-BMAP-28m treatment. myr-BMAP-28m induces mitochondrial membrane potential changes in prostate cancer PC3 and Du145 cells.

JC-1 fluorescence was red in the control group but green in the treated group, indicating increased mitochondrial membrane permeability, and this effect was concentration dependent (Fig. 4A). Laser confocal microscopy showed that the red fluorescently labeled mitochondria were concentrated at one pole of the cells after being labeled with the red fluorescent probe Rhodamine 123 (RHO123) (Fig. 4B). Fitc-labeled myr-BMAP-28m was distributed in the cytoplasm and co-localized with mitochondria, and the amount of co-localization was significantly higher than that of the BMAP-28m-treated group (Fig. 4C). Moreover, the intracellular ATP content was significantly decreased after myr-BMAP-28m treatment, and the decrease was more significant than that of BMAP-28m treatment. Fluorescence imaging and quantitative analysis showed that lipid ROS levels were significantly increased in Du145 and PC3 cells after treatment with myr-BMAP-28m (Fig. 4D). Furthermore, myr-BMAP-28m increased total ROS levels in a concentration dependent manner in both cell lines. Transmission electron microscopy results showed that the mitochondrial morphology of PC3 cells changed significantly after treatment with myr-BMAP-28m, indicating a significant mitochondrial damage effect (Fig. 4E).

5. Anticancer activity of myr-BMAP-28m against prostate tumors in vivo

The anticancer effect of myr-BMAP-28m was evaluated in the PC3 xenograft mouse model. All animals survived throughout the experiment and no significant weight loss was observed in myr-BMAP-28m-treated or BMAP-28M-treated mice compared with the control group (Fig. 5A). In contrast, xenograft tumor growth was significantly inhibited in the myr-BMAP-28m-treated group compared with the BMAP-28m-treated group (Fig. 5B). In addition, tumor samples from the control and experimental groups, as well as mouse heart, liver, spleen, lung, and kidney were analyzed by H&E staining and compared with the control group. The tumor tissues in the experimental group were structurally similar to those in the control group, and no obvious structural differences were observed in the internal organs of the three groups of mice (Fig. 5D-E). Therefore, it can be concluded that myr-BMAP-28m is not harmful to mouse tissues. After detection of cleaved Caspase-3 and Ki67 by immunohistochemistry (IHC), the results showed that the expression level of cleaved caspase-3 in the myr-BMAP-28m group was significantly higher than that in the BMAP-28m treatment group and the control group. However, the expression of Ki67 was significantly reduced (Fig. 5F-G).

(A–B) Body weight (A) and tumor volume (B) of nude mice bearing PC3 xenografts treated with vehicle control, BMAP-28m, myr-BMAP-28m, or Melittin for 25 days. (C) Final tumor weight at study endpoint. (D) Organ weights of heart, liver, lungs, kidney, and spleen at study endpoint, showing no significant treatment-related toxicity (ns, not significant). (E) Hematoxylin and eosin (H&E) staining of major organs and tumor tissues. No obvious histopathological damage was observed in vital organs, while tumor tissues showed significant necrosis and apoptosis in peptide-treated groups. Scale bar: 200 μm. (F) Immunohistochemical staining of Ki-67 (proliferation marker) and cleaved caspase-3 (apoptosis marker) in tumor tissues. (G) Quantification of immunohistochemical staining, showing reduced proliferation and increased apoptosis in peptide-treated tumors. (H) Schematic illustration of the proposed mechanism: myr-BMAP-28m binds to and disrupts the cancer cell membrane, leading to mitochondrial dysfunction (loss of membrane potential, ATP depletion, ROS accumulation), and activation of the intrinsic apoptotic

pathway via modulation of Bax/Bcl-2 and cleaved caspase-3 and PARP. Data are mean ± SD (n = 6). *P < 0.05, **P < 0.01, ***P < 0.001 vs. Ctrl.

Discussion

Antimicrobial peptides have become a research hotspot in the field of tumor therapy due to their broad-spectrum antibacterial activity and potential anti-tumor properties[21]. This study, through a series of in vitro and in vivo experiments, confirmed that myr-BMAP-28m exhibits superior performance in the treatment of prostate cancer. This section will conduct an in-depth discussion based on the experimental results, covering aspects such as cytotoxicity selectivity, cell cycle regulation and apoptosis induction mechanisms, cell membrane damage and mitochondrial targeting, as well as in vivo anti-tumor effects and safety, aiming to clarify the core advantages and potential action pathways of myr-BMAP-28m in the treatment of prostate cancer, and provide a theoretical basis for its subsequent clinical transformation (Fig. 5H).

One of the core requirements for tumor treatment drugs is to have good tumor cell selectivity toxicity, that is, to effectively kill tumor cells while minimizing damage to normal cells[22]. The results of this study show that compared with BMAP-28m, myr-BMAP-28m has significantly enhanced cytotoxicity against prostate cancer cells, while its cytotoxicity to normal cells is significantly reduced. This characteristic gives it a significant advantage in the treatment of prostate cancer.

The cytotoxicity differences of antimicrobial peptides are usually closely related to the differences in cell membrane structure[23]. Compared with normal cells, tumor cell membranes have features such as phosphatidylserine externalization, reduced cholesterol content, and higher surface negative charge density, which provide a basis for the targeted recognition and binding of antimicrobial peptides[23,24]. myr-BMAP-28m may enhance its binding affinity to the negative charge sites on the surface of prostate cancer cell membranes through N-terminal myristoylation modification, thereby improving its targeting to tumor cells. For normal cells, due to their relatively stable cell membrane structure and lower negative charge density, the binding ability of myr-BMAP-28m is weaker, resulting in lower toxicity. In contrast, the unmodified BMAP-28m has lower specificity in recognizing cell membranes, leading to certain toxicity to normal cells while killing tumor cells. This result suggests that myristoylation modification, by optimizing the cell membrane targeting of antimicrobial peptides, significantly improves the safety and effectiveness of tumor treatment, providing a new approach to solving the bottleneck problems of traditional chemotherapy drugs.

Disordered cell cycle and apoptosis inhibition are the core biological characteristics of tumor cell unlimited proliferation. Therefore, drugs that can effectively regulate the cell cycle of tumor cells and induce their apoptosis often have good anti-tumor activity[25,26]. This study found that myr-BMAP-28m can arrest the cell cycle of prostate cancer cells in the G1 phase and significantly induce apoptosis, accompanied by an increase in the expression levels of apoptosis-related proteins. This result reveals an important mechanism of its anti-tumor effect. The G1 phase is the initial stage of the cell cycle and a key

period for cell growth and DNA damage repair. Arresting the cell cycle in the G1 phase can effectively inhibit tumor cells from entering the S phase for DNA replication, thereby blocking their proliferation process[27,28]. At the same time, the induction of apoptosis further enhances its anti-tumor effect. The increase in the expression of apoptosis-related proteins (such as Bax, Caspase-3, etc.) induces apoptosis in prostate cancer cells[29]. Compared with BMAP-28m, myr-BMAP-28m has a stronger effect in blocking the cell cycle and a higher efficiency in inducing apoptosis, with a more significant increase in the expression of apoptosis-related proteins. In addition, the high selectivity toxicity of myr-BMAP-28m enables it to effectively kill tumor cells without significantly affecting the cell cycle process and apoptosis state of normal cells, further highlighting its clinical application potential.

The cell membrane is an important barrier of the cell. The damage to the cell membrane by antimicrobial peptides is one of the important ways for them to exert toxicity[30,31]. The myr-BMAP-28m binds to the prostate cancer cell membrane and creates pores, thereby destroying the integrity of the cell membrane and causing intracellular contents such as LDH to be released into the extracellular space, which in turn leads to cell death. Compared with BMAP-28m, myr-BMAP-28m causes a higher release of LDH, suggesting that it has a stronger damaging effect on the prostate cancer cell membrane. The damage to the cell membrane not only directly leads to the death of some tumor cells but also provides a channel for it to enter the cell and exert further regulatory effects (such as regulating the cell cycle, inducing apoptosis, and damaging mitochondria, etc.).

Mitochondria are the "powerhouses" of the cell and also an important regulatory center for cell apoptosis. Mitochondrial damage is a key step in inducing cell apoptosis[32]. This study confirmed the damaging effect of myr-BMAP-28m on prostate cancer cell mitochondria through experiments such as JC-1, ROS, RHO123, ATP determination, and scanning electron microscopy. The results of the JC-1 experiment showed that the mitochondrial membrane potential of prostate cancer cells significantly decreased after treatment with myr-BMAP-28m, indicating that the mitochondrial membrane structure was damaged; the increase in ROS levels indicated enhanced mitochondrial oxidative stress, which further led to mitochondrial functional damage; the change in RHO123 accumulation suggested an increase in mitochondrial membrane permeability; the decrease in ATP content indicated that the energy metabolism function of mitochondria was inhibited; and scanning electron microscopy observations further visually demonstrated the abnormal morphology of mitochondria. These experimental results collectively confirmed that myr-BMAP-28m can induce cell apoptosis by targeting and damaging mitochondria, thereby disrupting their structure and function.

myr-BMAP-28m can effectively inhibit the growth of prostate tumors in vivo, with tumor volume and weight significantly smaller than those of the control group and the BMAP-28m treatment group, suggesting that its in vivo anti-tumor activity is superior to that of BMAP-28m. This result is consistent with the in vitro experimental results, confirming the stability and reliability of the anti-tumor effect of myr-BMAP-28m. The IHC experimental results provided direct evidence for the in vivo anti-tumor mechanism of myr-BMAP-28m. The increased expression of apoptosis-related proteins and the decreased expression of proliferation-related proteins in tumor tissues indicated that myr-BMAP-28m

can also exert anti-tumor effects in vivo by inducing tumor cell apoptosis and inhibiting tumor cell proliferation, which is completely consistent with the mechanism revealed in the in vitro experiments. This result indicates that myr-BMAP-28m can exert anti-tumor effects through the same core mechanism both in vitro and in vivo, and its mechanism of action has good consistency and stability.

This study systematically explored the anti-prostate cancer effect and mechanism of myr-BMAP-28m through in vitro cell experiments and in vivo animal experiments, and made a comprehensive comparison with BMAP-28m. The results showed that myr-BMAP-28m has significant advantages. These advantages of myr-BMAP-28m all stem from its N-terminal myristoylation modification, which optimizes the core links of its anti-tumor effect by enhancing its binding ability to the tumor cell membrane, membrane perforation efficiency, and intracellular transport ability.

Although this study has achieved positive results, there are still some shortcomings. Through further in-depth research in the future, it is expected to further improve the anti-tumor mechanism of myr-BMAP-28m, provide more theoretical support for its clinical transformation, and make it a potential new drug for the treatment of prostate cancer.

Statistical Analysis

All experiments were repeated at least three times. Results are expressed as the mean ± standard error (mean ± SE). The significance of differences between treatments and their respective controls was determined by Student's t-test. A P value < 0.05 was considered statistically significant.

Declarations

Conflict of Interest

The authors declare that the research was conducted in the absence of any commercial or financial relationships that could be construed as a potential conflict of interest.

Competing interests

The authors declare no competing interests.

Funding

This research was funded by grants from the National Natural Science Foundation of China (Grant No.82260493).

Author Contribution

MS: Conceptualization, methodology, investigation, supervision, writing-review and editing. YBZ: formal analysis, investigation, validation, writing-original draft. MQZ: formal analysis, investigation, validation, writing-original draft. YML: writing-original draft. MJL: formal analysis, writing-original draft, funding acquisition. YYH: Conceptualization, writing-review and editing, supervision, project administration, funding acquisition.

References

1. Siegel RL, Kratzer TB, Giaquinto AN, Sung H, Jemal A (2025) Cancer statistics, 2025. CA Cancer J Clin 75(1):10–45. 10.3322/caac.21871
2. Eder IE, Haag P, Bartsch G, Klocker H (2005) Targeting the androgen receptor in hormone-refractory prostate cancer–new concepts. Future Oncol 1(1):93–101. 10.1517/14796694.1.1.91
3. Teo MY, Rathkopf DE, Kantoff P (2019) Treatment of Advanced Prostate Cancer. Annu Rev Med 70:479–499. 10.1146/annurev-med-051517-011947
4. Puhr M, Hoefer J, Schäfer G et al (2012) Epithelial-to-mesenchymal transition leads to docetaxel resistance in prostate cancer and is mediated by reduced expression of miR-200c and miR-205. Am J Pathol 181(6):2188–2201. 10.1016/j.ajpath.2012.08.011
5. Rr JM (2010) NCCN clinical practice guidelines in oncology: prostate cancer. J Natl Compr Cancer Network: JNCCN 8(2). 10.6004/jnccn.2010.0012
6. Holohan C, Van Schaeybroeck S, Longley DB, Johnston PG (2013) Cancer drug resistance: an evolving paradigm. Nat Rev Cancer 13(10):714–726. 10.1038/nrc3599
7. U M, Ra G, Ma M et al (2021) The tumor microenvironment as driver of stemness and therapeutic resistance in breast cancer: New challenges and therapeutic opportunities. Cell Oncol (Dordrecht Netherlands) 44(6). 10.1007/s13402-021-00634-9
8. Otvos L (2017) Host Defense Peptides and Cancer; Perspectives on Research Design and Outcomes. Protein Pept Lett 24(10):879–886. 10.2174/0929866524666170202153501
9. Zhang QY, Yan ZB, Meng YM et al (2021) Antimicrobial peptides: mechanism of action, activity and clinical potential. Mil Med Res 8(1):48. 10.1186/s40779-021-00343-2
10. Dong Z, Zhang X, Zhang Q et al (2024) Anticancer Mechanisms and Potential Anticancer Applications of Antimicrobial Peptides and Their Nano Agents. Int J Nanomed 19:1017–1039. 10.2147/IJN.S445333
11. Mwangi J, Hao X, Lai R, Zhang ZY (2019) Antimicrobial peptides: new hope in the war against multidrug resistance. Zool Res 40(6):488–505. 10.24272/j.issn.2095-8137.2019.062
12. Dong L, Li Y, Zhang Y, Su S (2025) Cationic antimicrobial peptide CC34 potential anticancer and apoptotic induction on cancer cells. Amino Acids 57(1):28. 10.1007/s00726-025-03458-1

13. Baxter AA, Lay FT, Poon IKH, Kvansakul M, Hulett MD (2017) Tumor cell membrane-targeting cationic antimicrobial peptides: novel insights into mechanisms of action and therapeutic prospects. Cell Mol Life Sci 74(20):3809–3825. 10.1007/s00018-017-2604-z
14. Sh HL (2023) Rationally designed PMAP-23 derivatives with enhanced bactericidal and anticancer activity based on the molecular mechanism of peptide-membrane interactions. Amino Acids 55(8). 10.1007/s00726-023-03290-5
15. He T, Qu R, Zhang J (2022) Current synthetic chemistry towards cyclic antimicrobial peptides. J Pept Sci 28(6):e3387. 10.1002/psc.3387
16. Bucataru C, Ciobanasu C (2024) Antimicrobial peptides: Opportunities and challenges in overcoming resistance. Microbiol Res 286:127822. 10.1016/j.micres.2024.127822
17. Bellavita R, Braccia S, Galdiero S, Falanga A (2023) Glycosylation and Lipidation Strategies: Approaches for Improving Antimicrobial Peptide Efficacy. Pharmaceuticals 16(3):439. 10.3390/ph16030439
18. F B FM (2022) Design and Characterization of Myristoylated and Non-Myristoylated Peptides Effective against Candida spp. Clin Isolates Int J Mol Sci 23(4). 10.3390/ijms23042164
19. Y L, S L, T S, et al. N-terminal Myristoylation Enhanced the Antimicrobial Activity of Antimicrobial Peptide PMAP-36PW. Frontiers in cellular and infection microbiology. (2020) ;10. 10.3389/fcimb.2020.00450
20. C L (2018) N-myristoylation of Antimicrobial Peptide CM4 Enhances Its Anticancer Activity by Interacting With Cell Membrane and Targeting Mitochondria in Breast Cancer Cells. Front Pharmacol 9. 10.3389/fphar.2018.01297
21. Erdem Büyükkiraz M, Kesmen Z (2022) Antimicrobial peptides (AMPs): A promising class of antimicrobial compounds. J Appl Microbiol 132(3):1573–1596. 10.1111/jam.15314
22. Qq JW (2014) Selective tumor cell killing by triptolide in p53 wild-type and p53 mutant ovarian carcinomas. Med Oncol (Northwood Lond Engl) 31(7). 10.1007/s12032-014-0014-8
23. Vona R, Iessi E, Matarrese P (2021) Role of Cholesterol and Lipid Rafts in Cancer Signaling: A Promising Therapeutic Opportunity? Front Cell Dev Biol 9:622908. 10.3389/fcell.2021.622908
24. Wodlej C, Riedl S, Rinner B et al (2019) Interaction of two antitumor peptides with membrane lipids - Influence of phosphatidylserine and cholesterol on specificity for melanoma cells. PLoS ONE 14(1):e0211187. 10.1371/journal.pone.0211187
25. Bai M, Papoudou-Bai A, Kitsoulis P et al (2005) Cell cycle and apoptosis deregulation in classical Hodgkin lymphomas. Vivo 19(2):439–453
26. Hanahan D, Weinberg RA (2011) Hallmarks of cancer: the next generation. Cell 144(5):646–674. 10.1016/j.cell.2011.02.013
27. Du J, Chen C, Sun Y, Zheng L, Wang W (2015) Ponicidin suppresses HT29 cell growth via the induction of G1 cell cycle arrest and apoptosis. Mol Med Rep 12(4):5816–5820. 10.3892/mmr.2015.4150

28. Xiong Y, Li T, Assani G et al (2019) Ribociclib, a selective cyclin D kinase 4/6 inhibitor, inhibits proliferation and induces apoptosis of human cervical cancer in vitro and in vivo. Biomed Pharmacother 112:108602. 10.1016/j.biopha.2019.108602
29. Phongsuwichetsak C, Suksrichavalit T, Chatupheeraphat C, Eiamphungporn W, Yainoy S, Yamkamon V (2024) Diospyros rhodocalyx Kurz induces mitochondrial-mediated apoptosis via BAX, Bcl-2, and caspase-3 pathways in LNCaP human prostate cancer cell line. PeerJ 12:e17637. 10.7717/peerj.17637
30. Agadi N, Maity A, Jha AK, Chakrabarti R, Kumar A (2022) Distinct mode of membrane interaction and disintegration by diverse class of antimicrobial peptides. Biochim Biophys Acta Biomembr 1864(12):184047. 10.1016/j.bbamem.2022.184047
31. Lee J, Lee DG (2015) Antimicrobial Peptides (AMPs) with Dual Mechanisms: Membrane Disruption and Apoptosis. J Microbiol Biotechnol 25(6):759–764. 10.4014/jmb.1411.11058
32. Dadsena S, Zollo C, García-Sáez AJ (2021) Mechanisms of mitochondrial cell death. Biochem Soc Trans 49(2):663–674. 10.1042/BST20200522

Figures

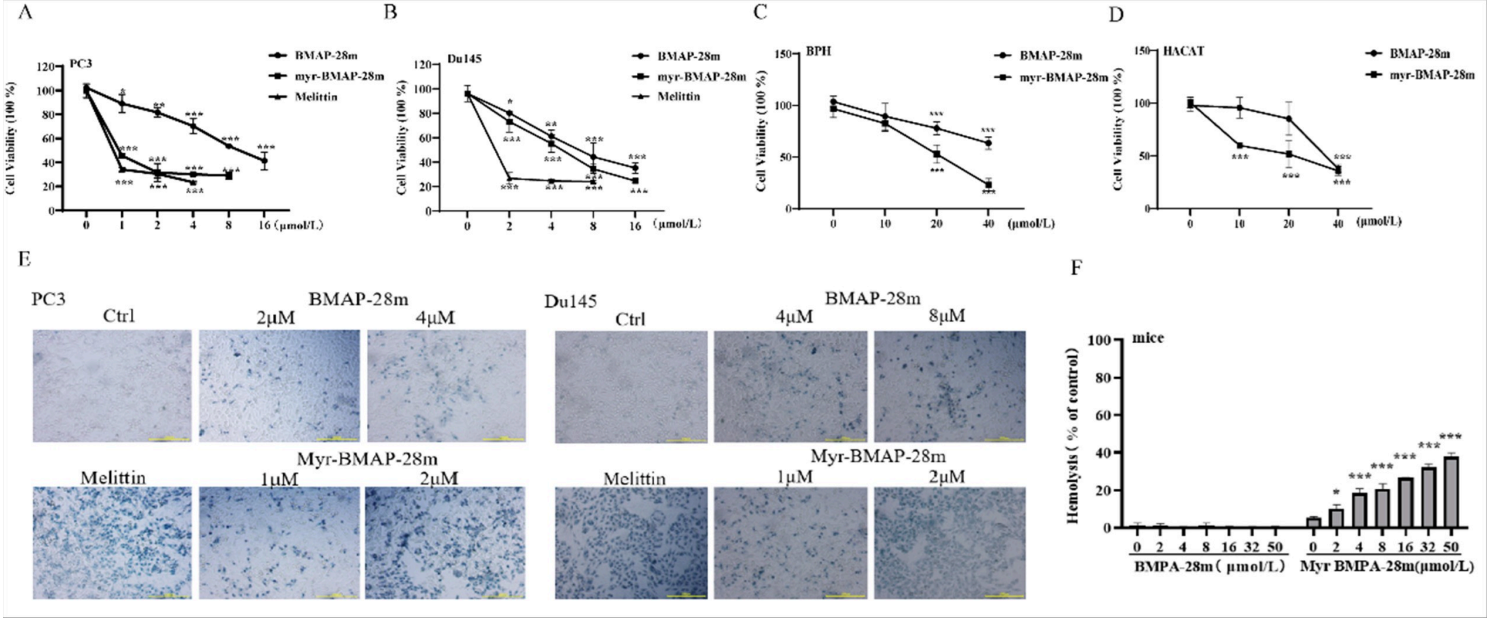


Figure 1

Effects of BMAP-28m and myr-BMAP-28m on the viability of tumor cells and normal cells.

(A–D) CCK-8 assays showing dose-dependent viability of PC3 (A), Du145 (B), BPH-1 (C), and HACAT (D) cells after 24 h treatment with peptides (0–16 μmol/L). *n=3, *P<0.05, **P<0.01, ***P<0.001 vs. ctrl. (E) Transwell migration assays of PC3 and Du145 cells treated with peptides, showing reduced migration in a concentration-dependent manner. Scale bar: 200 μm. (F) In vivo antitumor efficacy of BMAP-28m and

myr-BMAP-28m in PC3 xenografts. Tumor volume (% of control) after i.v. administration every 3 days for 21 days. *n=6, *P<0.05, **P<0.01, ***P<0.001.

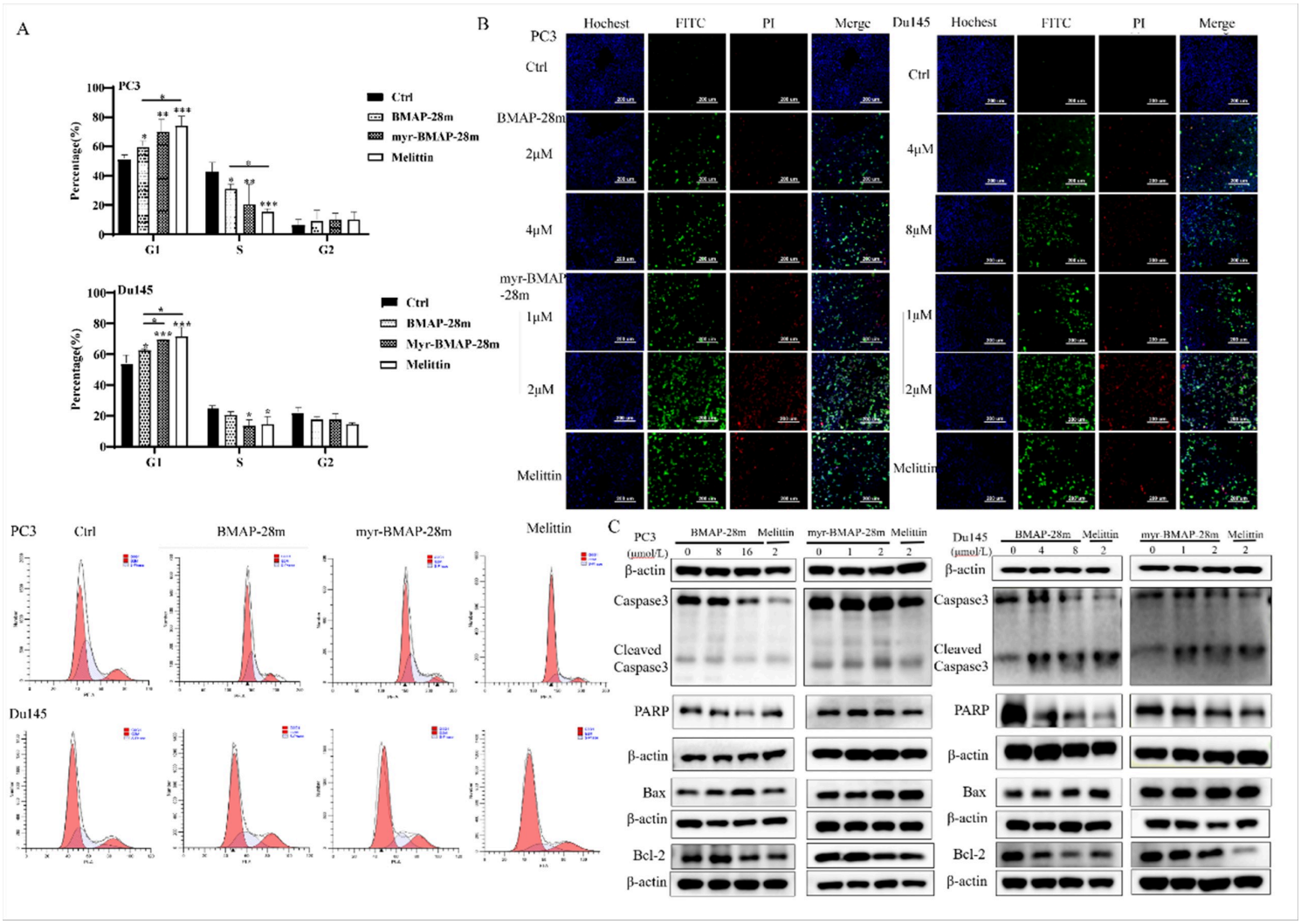


Figure 2

BMAP-28m and myr-BMAP-28m induce cell cycle arrest, apoptosis, and activation of apoptotic signaling pathways in prostate cancer cells

(A) Flow cytometry analysis of cell cycle distribution in PC3 and Du145 cells after 24 hh of treatment with BMAP-28m, myr-BMAP-28m, or Melittin. The bar graph shows the percentage of cells in the G1, S, and G2 phases. Data are presented as mean ± standard deviation (n=3). Representative flow cytometry plots below show changes in the cell cycle following peptide treatment. (B) Representative fluorescence microscopy images of PC3 and Du145 cells after peptide treatment stained with Hoechst/Annexin V-FITC/PI triple staining. Hoechst (blue) labels all nuclei, FITC (green) marks phosphatidylserine externalization (early apoptosis), and PI (red) indicates late apoptosis/necrosis. The merged images show concentration-dependent apoptotic progression. Scale bar: 200 μm. (C) Western blot analysis of the expression of key apoptotic proteins in PC3 and Du145 cells after peptide treatment. *Statistical significance: *P < 0.05; **P < 0.01; ***P < 0.001.

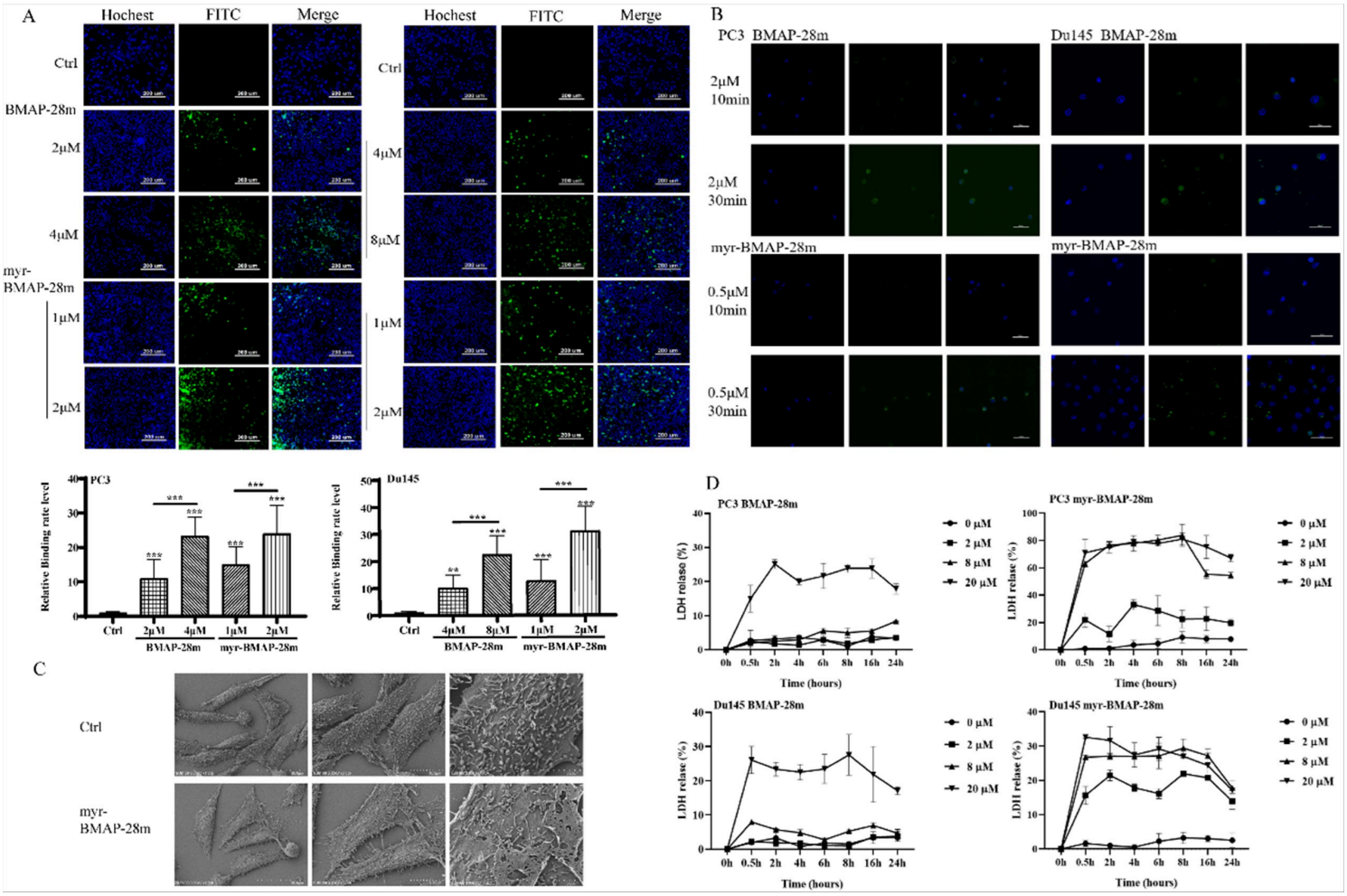


Figure 3

BMAP-28m and myr-BMAP-28m Induce Membrane Damage and Permeability Changes in Prostate Cancer Cells

(A) Representative high-content fluorescence images of PC3 and Du145 cells stained with Hoechst/FITC-BMAP-28m or myr-BMAP-28m after treatment with different concentrations of BMAP-28m or myr-BMAP-28m. Hoechst (blue) labels all nuclei, while FITC-BMAP-28m or myr-BMAP-28m (green) indicates the distribution of antimicrobial peptides in cells. The bar graphs represent the relative binding level of the peptides to PC3 and Du145 cell membranes based on fluorescence quantification from high-content images. Data are expressed as mean ± standard deviation (n=15). (B) Fluorescence intensity and distribution captured by laser confocal microscopy after PC3 and Du145 cells were treated with FITC-BMAP-28m / myr-BMAP-28m for different times. (C) Scanning electron microscopy (SEM) images of untreated (control) PC3 cells or cells treated with myr-BMAP-28m. Compared with the intact and smooth cell membranes of the control group, myr-BMAP-28m treatment caused significant membrane damage, including membrane blebbing, pore formation, and surface structure disruption.(D) Real-time lactate dehydrogenase (LDH) release assay after PC3 and Du145 cells were treated with different concentrations of BMAP-28m or myr-BMAP-28m for 24 h. *Statistical significance: *$P < 0.05$; **$P < 0.01$; ***$P < 0.001$.

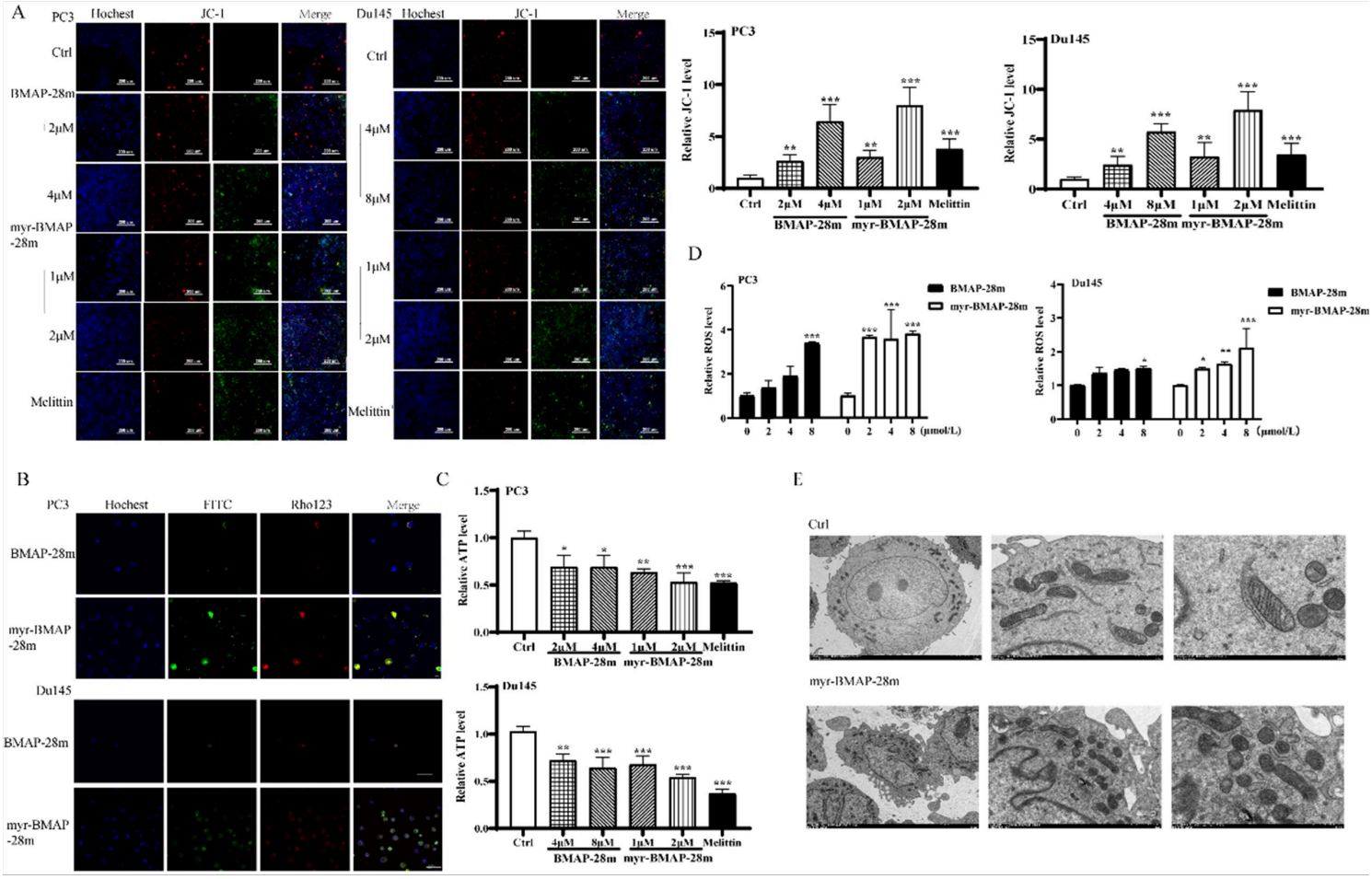


Figure 4

BMAP-28m and myr-BMAP-28m induce mitochondrial dysfunction in prostate cancer cells

(A) Representative high-content fluorescence images of PC3 and Du145 cells stained with Hoechst/JC-1 after treatment with BMAP-28m, myr-BMAP-28m, or Melittin. JC-1 aggregates (red) indicate intact mitochondrial membrane potential (ΔΨm), while JC-1 monomers (green) indicate mitochondrial membrane depolarization. The bar graph quantifies the relative intensity of JC-1 monomer/green fluorescence, showing a concentration-dependent loss of membrane potential. (B) Representative confocal images of PC3 and Du145 cells stained with Hoechst/FITC-Annexin V/Rhodamine 123 after peptide treatment. Rhodamine 123 (red) labels mitochondria with intact membrane potential, further confirming the decline in mitochondrial membrane potential. Scale bar: 200 μm.(C) Relative ATP levels in PC3 and Du145 cells after peptide treatment (measured by luminescence). Results show a significant reduction in cellular ATP content, indicating impaired mitochondrial energy metabolism. (D) Levels of reactive oxygen species (ROS) generation in PC3 and Du145 cells after peptide treatment (quantified by DCFH-DA fluorescence). myr-BMAP-28m induces higher ROS accumulation than BMAP-28m, suggesting stronger oxidative stress. (E) Transmission electron microscopy (TEM) images of PC3 cells untreated (control) or treated with myr-BMAP-28m. Compared with the control group, where mitochondria display intact structure and clear cristae, myr-BMAP-28m treatment results in severe mitochondrial damage,

including cristae rupture, swelling, and vacuolization. Scale bar: 500 nm. *Statistical significance: *P < 0.05; **P < 0.01; ***P < 0.001.

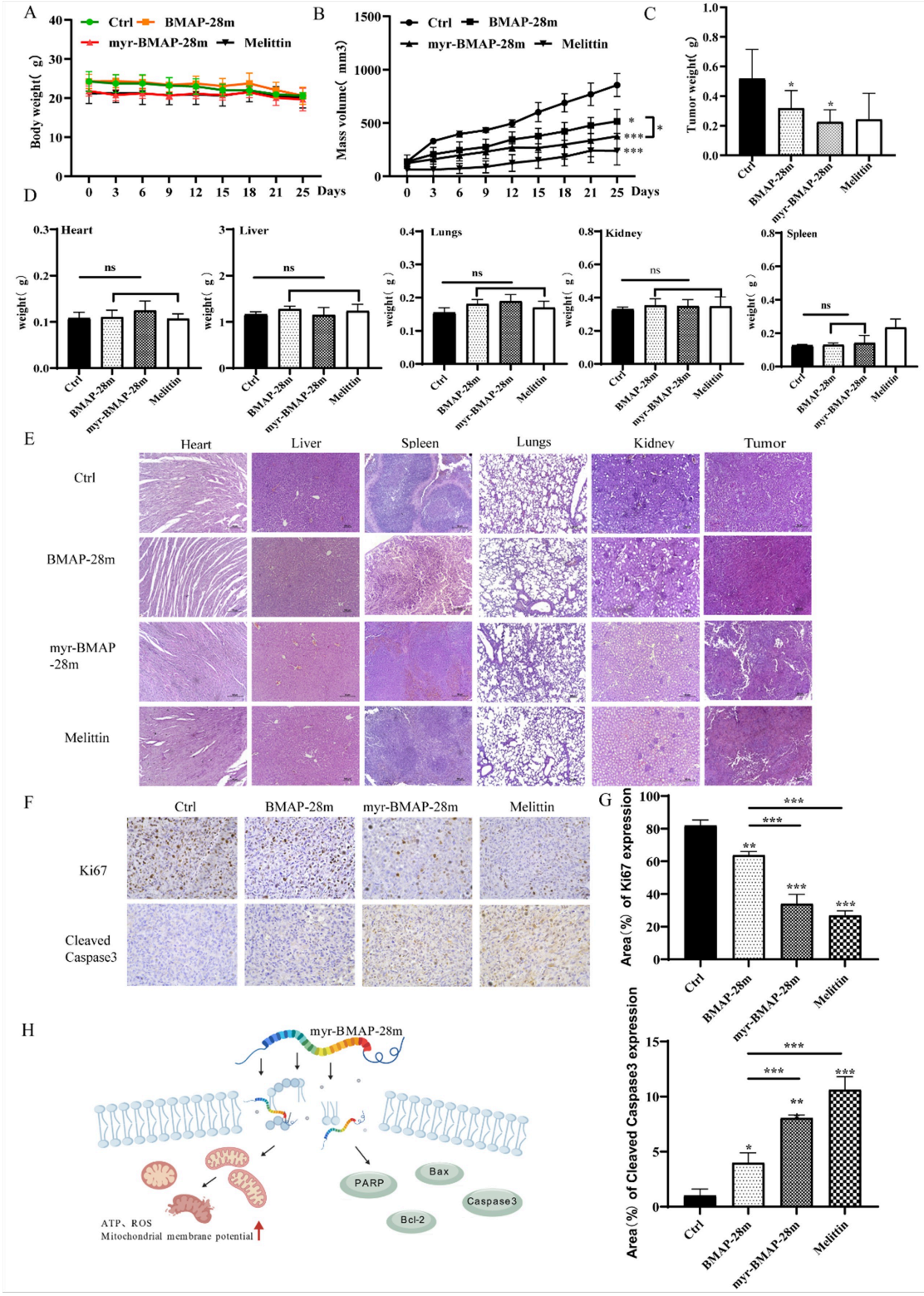


Figure 5

In vivo antitumor efficacy, safety, and proposed mechanism of action of BMAP-28m and myr-BMAP-28m.

(A–B) Body weight (A) and tumor volume (B) of nude mice bearing PC3 xenografts treated with vehicle control, BMAP-28m, myr-BMAP-28m, or Melittin for 25 days. (C) Final tumor weight at study endpoint. (D) Organ weights of heart, liver, lungs, kidney, and spleen at study endpoint, showing no significant treatment-related toxicity (ns, not significant). (E) Hematoxylin and eosin (H&E) staining of major organs and tumor tissues. No obvious histopathological damage was observed in vital organs, while tumor tissues showed significant necrosis and apoptosis in peptide-treated groups. Scale bar: 200 μm. (F) Immunohistochemical staining of Ki-67 (proliferation marker) and cleaved caspase-3 (apoptosis marker) in tumor tissues. (G) Quantification of immunohistochemical staining, showing reduced proliferation and increased apoptosis in peptide-treated tumors. (H) Schematic illustration of the proposed mechanism: myr-BMAP-28m binds to and disrupts the cancer cell membrane, leading to mitochondrial dysfunction (loss of membrane potential, ATP depletion, ROS accumulation), and activation of the intrinsic apoptotic pathway via modulation of Bax/Bcl-2 and cleaved caspase-3 and PARP. Data are mean ± SD (n=6). *P < 0.05, **P < 0.01, ***P < 0.001 vs. Ctrl.

Supplementary Files

This is a list of supplementary files associated with this preprint. Click to download.

- Supplementaryfigure.docx